Diagnosing Vibration Problems with Embedded Sensitivity Functions

Chulho Yang and **Douglas E. Adams,** Purdue University, West Lafayette, Indiana

Sung-Woo Yoo, ArvinMeritor, Columbus, Indiana

   When noise or vibration problems occur in mechanical systems, NVH (Noise, Vibration, Harshness) engineers often need to determine which component in the system is to blame and how to fix the problem through a design modification. The design challenge is that changes to a system may help to reduce a problem in one frequency range while simultaneously introducing another more serious problem in a different frequency range. One technique for diagnosing vibration and structure borne noise problems is described here whereby 'embedded' sensitivity functions are calculated directly from frequency response function (FRF) measurements. These sensitivity functions indicate which changes in mass, damping or stiffness will suppress vibration problems without introducing other problems. In so doing, the sensitivities circumvent the often poorly conditioned inverse problem. An application involving an exhaust subsystem is discussed after the embedded sensitivity functions are derived.

   System-level vibrations occur when mechanical subsystems are connected and then made to oscillate. As an example of a system-level vibration phenomenon, consider what happens when the static stiffness of a vehicle suspension in a standard model automobile is increased to produce a sportier new model. A change in the suspension can shift many or all of the standard vehicle resonant vibration frequencies to undesirable locations (e.g., power train harmonics). In this type of scenario, modifications to other components like the exhaust subsystem and engine/powertrain mounting subsystems must be made in addition to those in the suspension to avoid system-level vibration problems. Because there are an infinite number of design modifications from which to choose, it is very challenging for suppliers to decide how to change their components to most effectively address vibration and noise problems. Furthermore, suppliers rarely have models of all the relevant subsystems and often are not even certain which components are involved in the problem. In the absence of full system models shared among suppliers and vehicle manufacturers, prototypes are usually fabricated and tested in a costly and time-consuming iterative process to reduce noise and vibration levels in the frequency range of interest.

   The hybrid experimental-analytical approach discussed here aims to diagnose system-level vibration problems by using input-output measurements in conjunction with an appropriate lumped-parameter analytical representation of the system (i.e., parameterization). The technique calculates the sensitivity of a given vibration phenomenon to a component design parameter (mass, damping, stiffness) in a certain frequency range by combining input-output frequency response function (FRF) measurements in a special way. Specifically, FRFs in the full system are first measured and then combined to provide the desired sensitivity functions to perturbations in design parameters over which suppliers generally have some control. This embedded sensitivity technique is less expensive and faster to implement than an iterative approach and can work backwards from system-level measurements (hence the term 'embedded') to help identify the most promising design modifications given limited amounts of data.

   This 'top-down' embedded sensitivity technique is the reverse of the 'bottom-up' methods (including impedance mod-

eling, sub-structuring and component-mode synthesis) in the sense that system-level input-output measurements are used to quantify the significance of subsystem changes on overall system vibration characteristics. The work begins by deriving the mass, damping and stiffness sensitivity functions for a linear single degree-of-freedom (SDOF) vibrating system in order to demonstrate the subtle but important embedded nature of these functions. Then the SDOF system results are generalized to multiple degree-of-freedom (MDOF) systems. A case study involving an exhaust subsystem is then discussed to illustrate how sensitivity functions can be used to quantify the effectiveness of various parametric design modifications on specific NVH characteristics involving a particular vibration resonance problem. Previous studies involving sensitivity analysis in dynamic structures were based on substructure-coupling or impedance modeling concepts,[1-4] and most research in this area has focused on the sensitivity of eigenvalues and eigenvectors to changes in the system.[5-9] The work by Vanhonaker[10] may have been the first to provide a similar matrix formulation to that of the embedded sensitivity functions given here. The work presented here develops a sensitivity analysis technique for forced vibration response using limited frequency response input-output data. For more details on the approach for use with operating data and nonlinear systems refer to Yang et al.[11,12]

Embedded Sensitivity Theory

   Frequency response functions (FRFs) are used here to derive embedded sensitivity functions because FRFs are commonly measured and computed analytically/numerically to diagnose noise and vibration problems in many applications. These sensitivity functions indicate the variation in frequency response magnitude and phase with respect to perturbations in mass, damping and stiffness parameters. The term 'embedded' is used in this article to refer to the sensitivity functions because they are explicit functions of the FRFs, thus the individual mass, damping and stiffness parameters are not needed to compute the sensitivity functions.

   Single Degree-of-Freedom Derivation. To illustrate the derivation of embedded sensitivity functions, first consider the linear time-invariant single DOF system model shown in Figure 1. The linear, second order, ordinary differential equation of motion associated with this model is given by

$$M_1\ddot{y}_1 + C_1\dot{y}_1 + K_1 y_1 = f_1(t) \qquad (1)$$

where M_1, K_1 and C_1 are the mass, equivalent viscous damping and stiffness parameters, f_1 is the force excitation and y_1 is the displacement response with respect to the equilibrium position. To reiterate, the embedded sensitivity functions to be derived below should describe how the steady-state input-output relationship between f_1 and y_1 varies in both magnitude and phase as either M_1, K_1 or C_1 is made to vary.

   The corresponding FRF between f_1 and y_1, which is found by taking the ratio of the Fourier transform of the harmonic response to that of the excitation, is given by the familiar formula:

$$\frac{Y_1(\omega)}{F_1(\omega)} = H_1(\omega) = \frac{1}{K_1 - \omega^2 M_1 + j\omega C_1} \qquad (2)$$

The first parameter for which a sensitivity function will be found is the stiffness K_1. In order to provide some insight into the nature of this stiffness sensitivity function, plots of the magnitude and phase of $H_1(\omega)$ as functions of frequency are
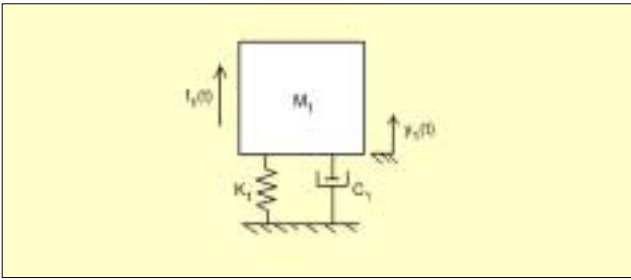
Figure 1. Schematic of a single degree-of-freedom linear system model.
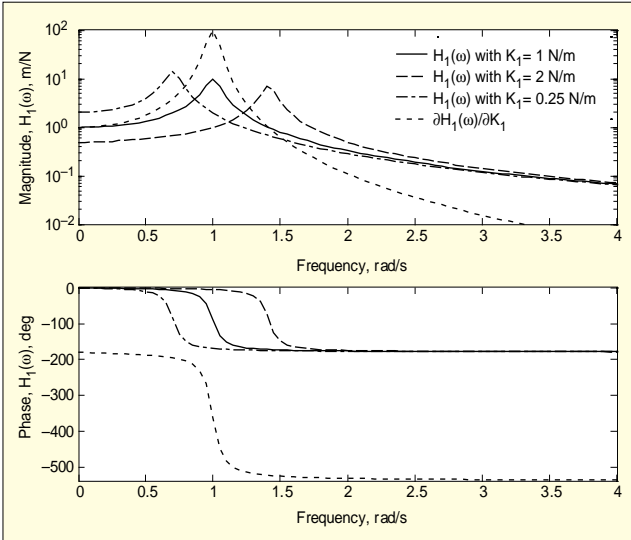

Figure 2. Magnitude (upper) and phase (lower) plots of single degree-of-freedom frequency response function for three values of K_1 with the corresponding embedded sensitivity function $\partial H_1/\partial K_1$ for the system stiffness parameter.

shown in Figure 2 for three different values of K_1 with fixed $M_1 = 1$ kg and $C_1 = 0.1$ N·s/m. These plots are not surprising because they simply show that increases in K_1 cause the undamped natural frequency $\omega_n = \sqrt{K_1/M_1}$ to increase and also cause the low frequency static stiffness line in the magnitude plot to decrease as $1/K_1$. These three plots also show that stiffness has little effect on the response for high frequencies where inertia forces dominate. The sensitivity function that is derived below gives similar indications.

The sensitivity of the FRF in Equation 2 to variations in stiffness K_1 is found by taking the partial derivative of $H_1(\omega)$ with respect to K_1 as follows:

$$\frac{\partial H_1(\omega)}{\partial K_1} = \frac{-1}{(K_1 - \omega^2 M_1 + j\omega C_1)^2} = -H_1^2(\omega) \qquad (3)$$

Note that after the partial derivative is taken the resulting sensitivity function can be expressed explicitly in terms of the FRF, $H_1(\omega)$, and does not require knowledge of any of the system parameters within the model. The only requirement in taking the partial derivatives was that the lumped parameter form be known. Furthermore, this type of parameterization is often known or can be found easily in practical applications of the type envisioned by this research.

Plots of the magnitude and phase of $\partial H_1/\partial K_1$ as functions of frequency are shown in Figure 2 overlaid with the FRFs for three different values of the stiffness parameter. Note that the sensitivity function clearly indicates that variations in stiffness do not significantly affect the high frequency portion of the FRF in magnitude or in phase. The high sensitivity near the peak of the FRF is also reflected in the plot, as is the uniform decrease in the low frequency portion of the FRF. The mass and damping sensitivity functions are derived below in Equations 4 and 5 and can also be interpreted in similar ways as for the stiffness sensitivity function. In particular, the embedded sensitivity functions indicate that the SDOF FRF is most sensitive
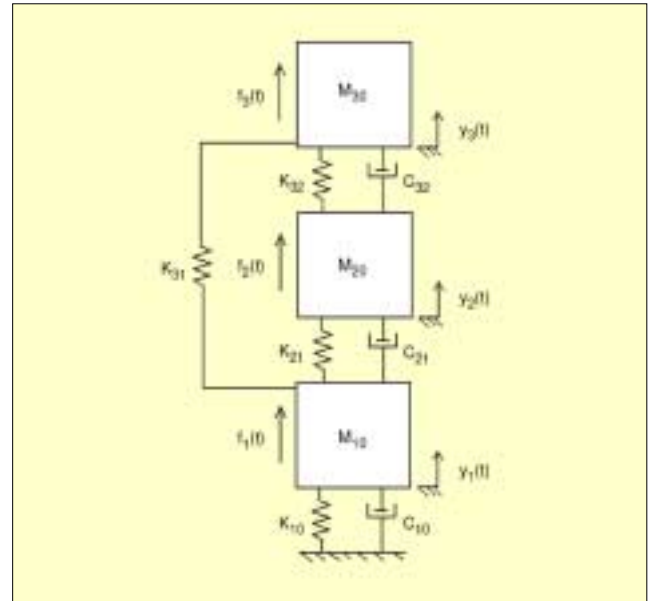

Figure 3. Schematic of a three degree-of-freedom linear system model with an alternative parameter labeling format used to emphasize coupling.

to damping in the frequency range surrounding the resonance peak and most sensitive to mass near the resonance peak and upper frequency range as expected.

$$\frac{\partial H_1(\omega)}{\partial C_1} = \frac{-j\omega}{(K_1 - \omega^2 M_1 + j\omega C_1)^2} = -j\omega H_1^2(\omega) \qquad (4)$$

$$\frac{\partial H_1(\omega)}{\partial M_1} = \frac{-\omega^2}{(K_1 - \omega^2 M_1 + j\omega C_1)^2} = \omega^2 H_1^2(\omega) \qquad (5)$$

Multi Degree-of-Freedom System Derivation. Although the SDOF example was interesting, it does not necessarily have much practical value for diagnosing system level vibration problems because they always involve more than one DOF. Fortunately, the technique used above to derive the embedded sensitivity functions for variations in mass, damping and stiffness in the SDOF case generalizes to higher order systems. The embedded sensitivity functions can be derived from inspection of higher DOF systems using a slightly modified set of system parameters.

Consider the linear three DOF system model shown in Figure 3. Note that the parameters in Figure 3 have been modified in order to emphasize the coupling within the system. In general, K_{jk} is the stiffness between DOFs k and j and the viscous damping coefficients are similarly defined. An index of '0' is used in the stiffness and damping parameters associated with the boundary condition K_{10} and C_{10} because the coupling in these cases is between ground and DOF 1. Also note that the mass parameters M_{j0} are all expressed with respect to ground because the inertial terms are defined with respect to the inertial reference frame. In systems like this one the sensitivity functions for $H_{jk}(\omega)$ can be found by extending the previous results. By carrying out the various sensitivity derivations, it can be shown that the general sensitivity functions of $H_{jk}(\omega)$ with respect to the coupling parameter (e.g., M_{m0}, C_{mn}, K_{mn}) are given by:

$$\frac{\partial H_{jk}}{\partial K_{mn}} = -\left[H_{jm}(\omega) - H_{jn}(\omega)\right] \cdot \left[H_{km}(\omega) - H_{kn}(\omega)\right]$$

with $H_{j0}(\omega) \equiv 0$

$$\frac{\partial H_{jk}}{\partial C_{mn}} = j\omega \cdot \frac{\partial H_{jk}}{\partial K_{mn}}$$

$$\frac{\partial H_{jk}}{\partial M_{m0}} = (j\omega)^2 \cdot \frac{\partial H_{jk}}{\partial K_{m0}}$$

(6a-c)

Figure 4. Photo of exhaust subsystem under investigation supported with elastic cords to approximate free-free boundary conditions.
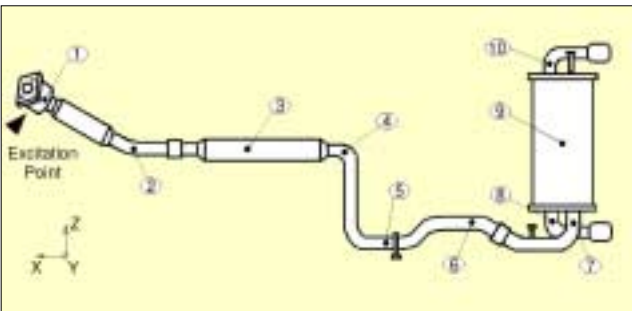

Figure 5. Illustration of measurement degrees-of-freedom used in tests on exhaust subsystem; triaxial acceleration measurements were made at each point.

For example, a few stiffness embedded sensitivity functions for $H_{11}(\omega)$ and $H_{32}(\omega)$ were found by substituting the necessary system-level FRFs directly into Equation 6a; the results are given below in Equations 7a-d:

$$\frac{\partial H_{11}}{\partial K_{10}} = -H_{11}^{2}(\omega) = -\left[H_{11}(\omega) - H_{10}(\omega)\right] \cdot \left[H_{11}(\omega) - H_{10}(\omega)\right]$$

where $H_{10}(\omega) = 0$

$$\frac{\partial H_{32}}{\partial K_{10}} = -H_{31}(\omega)H_{21}(\omega) \qquad \text{(7a-d)}$$

$$= -\left[H_{31}(\omega) - H_{30}(\omega)\right] \cdot \left[H_{21}(\omega) - H_{20}(\omega)\right]$$

$$\frac{\partial H_{32}}{\partial K_{21}} = -\left[H_{32}(\omega) - H_{31}(\omega)\right] \cdot \left[H_{22}(\omega) - H_{21}(\omega)\right]$$

Note that all of the stiffness sensitivity functions have the same form even though different combinations of $H_{jk}(\omega)$ appear in each expression. Similar results can be obtained using Equation 6b,c for mass and damping sensitivity functions.

Consider the stiffness sensitivity functions of $H_{31}(\omega)$ with respect to the series coupling stiffness K_{10} and the parallel coupling stiffness K_{31}. The series stiffness sensitivity function is the same form as Equation 6a and is given by

$$\frac{\partial H_{31}}{\partial K_{10}} = -H_{31}(\omega)H_{11}(\omega)$$

$$= -\left[H_{31}(\omega) - H_{30}(\omega)\right] \cdot \left[H_{11}(\omega) - H_{10}(\omega)\right] \qquad \text{(8)}$$

with $H_{30}(\omega) = 0 = H_{10}(\omega)$

The parallel stiffness sensitivity function is also given by the form in Equation 6a:

$$\frac{\partial H_{31}}{\partial K_{31}} = -\left[H_{33}(\omega) - H_{31}(\omega)\right] \cdot \left[H_{13}(\omega) - H_{11}(\omega)\right] \qquad \text{(9)}$$

These results are verified in the next section experimentally for an exhaust subsystem. The sensitivity functions are used

Figure 6. Electrodynamic shaker attached with stinger to front bracket of exhaust system in front of the bellows to simulate input from powertrain.
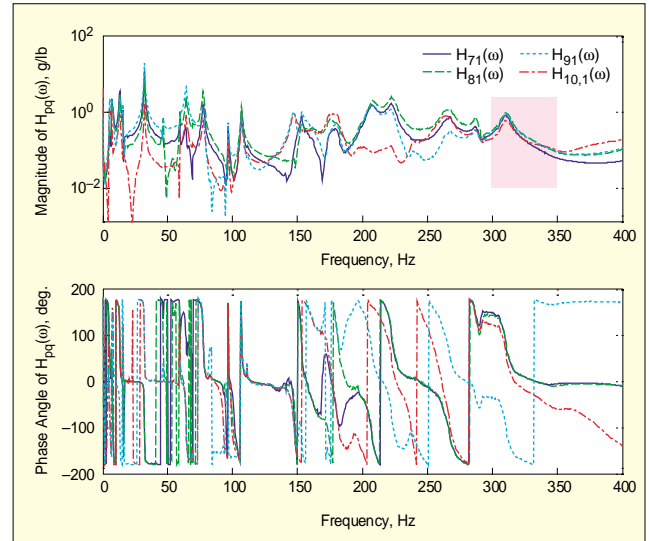

Figure 7. Magnitude (upper) and phase (lower) of y-direction frequency response functions with a skewed input.

to justify a design modification to the exhaust subsystem that mitigates a specific noise and vibration problem.

Application of Embedded Sensitivity Analysis

Embedded sensitivity functions are applied in this section to determine where and how an exhaust system design should be modified to most effectively remove a troublesome resonant frequency in the 300 to 350 Hz range without introducing other resonances in its place. The exhaust subsystem under investigation is shown in Figure 4. Note that the exhaust has been supported with elastic cords to approximate free-free boundary conditions by isolating the exhaust from the support frame.
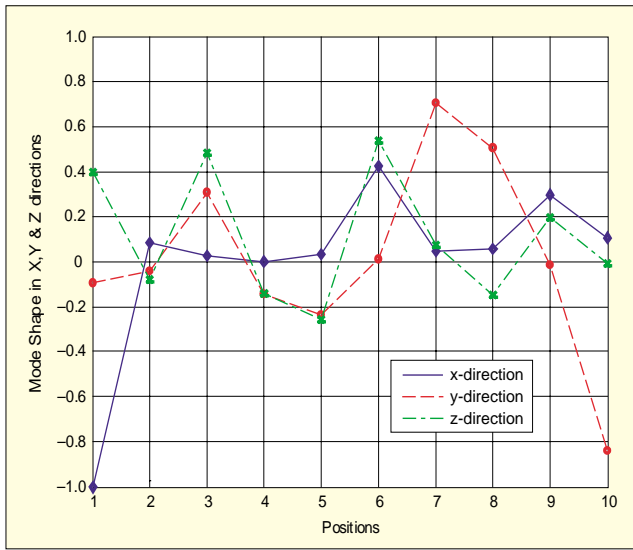
Figure 8. Relative deflection mode shapes in x-, y- and z-directions estimated using the imaginary parts (peak-pick method) of the associated FRFs (normalized).

Figure 9. Comparison of stiffness sensitivity functions of the exhaust system to changes near the bellows and the inlet muffler pipe.

The first generation design of this exhaust subsystem, which was installed in a standard compact vehicle model, did not exhibit a resonance problem in the 300 to 350 Hz range. However, when the suspension of the standard vehicle system was modified to produce a sportier model, a vibration problem in the rear floorboard of the newer model appeared with an accompanying structure-borne noise problem inside the saloon. Because the noise problem was introduced by a necessary change to the suspension system, a modification to the exhaust subsystem was required to mitigate the problem. In the course of evaluating potential design modifications, interesting observations were made regarding the effects of changes in the exhaust. After several unsuccessful design modifications were made, a successful modification to the muffler inlet pipe using a flexible Metex joint was identified. The discussion below is a follow-up analysis of that noise and vibration design scenario using embedded sensitivity functions.

Exhaust Subsystem Characteristics. The exhaust subsystem modal characteristics in the frequency range of interest were estimated using FRF measurements in the three Cartesian coordinate directions at ten locations (see Figure 5) not including the skewed driving point input location near the forward bracket of the exhaust (Figure 6). A 50 lb-f electrodynamic shaker was used, which was instrumented with a PCB 288D01 impedance head (sensitivity 102.24 mV/lbf, 98.36 mV/g) for measuring force and acceleration at the attachment location. This shaker excited the exhaust system into vibration to simulate the input from the powertrain and triaxial accelerometers (PCB model 356A08, sensitivity 92-102 mV/g, PCB model A356B18, sensitivity 907-1042 mV/g) were used to measure three axes of acceleration at each point in Figure 5. FRFs were computed using a Hanning window with 50% overlap signal processing, 4096 block size, 2048 Hz sampling frequency and a digital filter with a 800 Hz bandwidth for a 0.5 Hz frequency resolution.

FRFs in the three Cartesian coordinate directions were estimated for each input-output pair; the magnitude and phase of the y direction $H_{71}(\omega)$, $H_{81}(\omega)$, $H_{91}(\omega)$ and $H_{10,1}(\omega)$ FRFs are plotted in Figure 7. Note the peak in all three sets of FRFs near 312 Hz. The relative deflection mode shape associated with this particular damped modal frequency is shown in Figure 8 in all three directions. These shapes were obtained using the peak-pick modal parameter estimation method in which the imaginary portions of the associated FRFs $H_{n,1}(\omega)$ were taken to be the modal deflection coefficients at resonant peaks. This approach was valid near 312 Hz because that mode is dominant at that frequency. The first notable characteristic of this mode
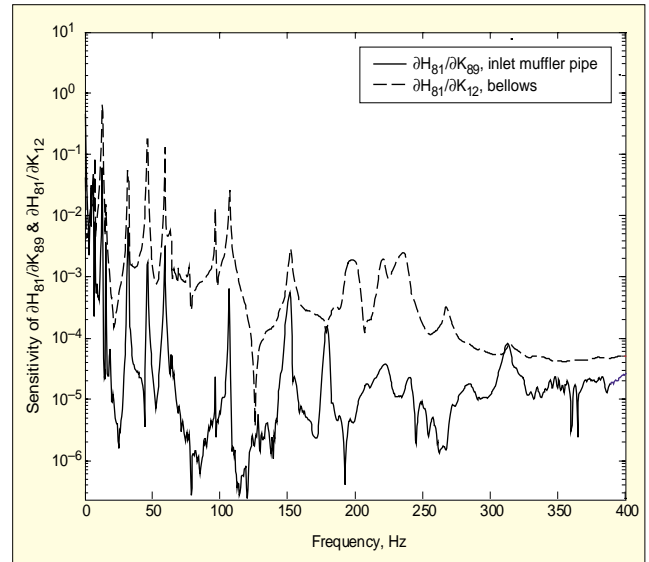
shape is that it has contributions from all three coordinate directions. Second, note that the x direction (longitudinal) mode shape has a rather large deflection at the input location compared to the other locations, indicating that the bellows, which is compliant in the x direction, isolates the exhaust system in that direction at that frequency. Third, note that the y direction (vertical) mode shape near 312 Hz exhibits a large relative deflection from the inlet pipe to the muffler across to the outlet pipe. This large torsional motion suggests that modifying the inlet to the muffler may shift this modal frequency out of the 300-350 Hz frequency range. However, the mode shape alone does not indicate what the ramifications are at other frequencies when shifting this mode. In contrast, embedded sensitivity functions do provide this type of information as shown below.

Embedded Sensitivity Analysis with Measured FRFs. As was previously mentioned, a change in the system at a frequency for which there is large relative motion will provide large changes at that frequency. However, there are two important pieces of information that are not obtained using this modal approach to examining design modifications:
1. The effects on frequencies/modes other than the problem frequency(ies)/mode(s);
2. The carry-over effects of lower frequencies on higher frequencies (e.g., static stiffness at the boundary condition).

Embedded sensitivity functions provide these other pieces of information because they are computed using all of the frequency response data rather than just the data at certain modes. The baseline and modified exhaust systems are now examined in light of the experimentally obtained embedded sensitivities to propose the most effective changes to the exhaust.

Recall that all three Cartesian directions of the unmodified exhaust system exhibited a significant mode in the 300-350 Hz range (approximately 312 Hz). In order to propose a design modification to the exhaust system that would affect this mode, several sets of embedded sensitivity functions were computed and examined. Initial results from the analytic model indicated that a change in the stiffness of the bellows could potentially help shift the 312 Hz mode out of the 300-350 Hz frequency range. The sensitivity function to stiffness changes towards the front of the exhaust system (path between points 1 and 2 in Figure 5) was computed using the following formulae:

$$\frac{\partial H_{81}}{\partial K_{12}} = -\left[H_{81}(\omega) - H_{82}(\omega) \right] \cdot \left[H_{11}(\omega) - H_{12}(\omega) \right] \qquad (10)$$

Note that the FRFs $H_{81}(\omega)$, $H_{11}(\omega)$, $H_{12}(\omega)$ and $H_{82}(\omega)$ were measured using impact testing for convenience as were the other

Figure 10. Photo of inlet pipe of muffler fitted with Metex joint for reducing the exhaust torsional coupling stiffness at that location to mitigate the vibration problem.

FRFs in the sensitivity functions below.

The sensitivity function of the same FRF, $H_{81}(\omega)$, to a stiffness change in the exhaust system at the inlet pipe to the muffler (path between points 8 and 9 in Figure 5) was also computed as follows:

$$\frac{\partial H_{81}}{\partial K_{89}} = -\Big[H_{88}(\omega) - H_{89}(\omega)\Big] \cdot \Big[H_{18}(\omega) - H_{19}(\omega)\Big] \quad (11)$$

When comparing these two sensitivity functions in Figure 9, note that changes at the muffler inlet pipe are more efficient than changes in the bellows at modifying/shifting the resonance near 312 Hz for two reasons. First, the magnitude of the sensitivity of $H_{81}(\omega)$ to K_{89} is relatively large at 312 Hz. Second, the sensitivity function for the change at the muffler inlet in other frequency ranges is small compared to the corresponding sensitivity function for the change in the bellows. Moreover, the change near the muffler has its greatest impact on vibration at 312 Hz whereas the change in the bellows makes a significant impact at many other frequencies as well. These broad changes are likely to create new vibration problems at other input frequencies of the powertrain.

These conclusions using embedded sensitivity functions were also confirmed with the experimentally determined FRFs for the exhaust system with a Metex joint inserted at the inlet pipe to the muffler (Figure 10). The FRFs in Figure 11 for the modified exhaust should be compared with the baseline FRFs given previously in Figure 7. Note that the peak in the neighborhood of 312 Hz has been shifted downward in frequency with the addition of the Metex joint. In other words, the vibration problem was effectively addressed by changing K_{89}.

Conclusions

The use of sensitivity analysis in diagnosing system-level vibration phenomena was examined in this article. Embedded sensitivity functions for one and higher degree-of-freedom systems were derived. It was shown that the resulting sensitivity functions were 'embedded' because they do not require explicit knowledge of the mass, damping or stiffness properties of a system, only the frequency response functions. Embedded sensitivity functions were then used to compare two different design modifications to an exhaust system bellows and muffler inlet pipe. It was shown that the muffler inlet modification was preferable for shifting the specific modal frequency near 312 Hz because that change did not introduce significant changes across the entire frequency range of interest as did the change to the bellows.
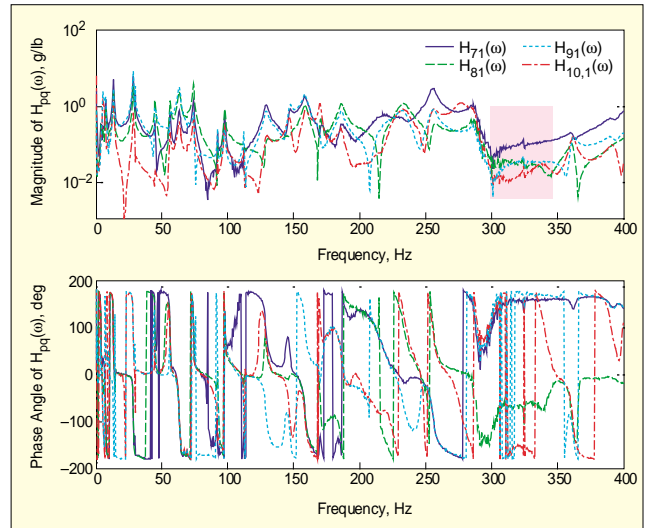

Figure 11. Magnitude (upper) and phase (lower) of y-direction FRFs of the modified exhaust with Metex joint.

References
1. Y. Yoshimura, "Design Sensitivity Analysis of Frequency Response in Machine Structures," *Journal of Mechanisms, Transmissions and Automation in Design*, 106, 119-125, 1984.
2. R. M. Lin, and D. J. Ewins, "Analytical Model Improvement Using Frequency Response Functions," *Mechanical Systems & Signal Processing*, V. 8, 437-458, 1994.
3. K.-J. Chang, and Y.-P. Park, "Structural Dynamic Modification Using Component Receptance," *Mechanical Systems & Signal Processing,* V. 12, 525-541, 1998.
4. B. R. Mace, and P. J. Shorter, "A Local Modal/Perturbational Method for Estimating Frequency Response Statistics of Built-Up Structures with Uncertain Properties," *Journal of Sound and Vibration,* V. 242, 793-811, 2001.
5. H. A. Jahn, "Improvement of an Approximate Set of Latent Roots and Modal Columns of a Matrix by Methods Akin to Those of Classical Perturbation Theory," *Quarterly Journal of Mechanics and Applied Mathematics*, V. 1, 132-144, 1948.
6. R. L. Fox, and M. P. Kapoor, "Rates of Change of Eigenvalues and Eigenvectors," *American Institute of Aeronautics and Astronautics Journal*, V. 6, 426-2429, 1968.
7. R. M. Lin and M. K. Lim, "Derivation of Structural Design Sensitivities from Vibration Test Data," *Journal of Sound & Vibration*, V. 201, 613-631, 1997.
8. Z.-Q. Qu, "Hybrid Expansion Method for Frequency Responses and their Sensitivities, Part I : Undamped Systems," *Journal of Sound & Vibration,* V. 231, 175-193, 2000.
9. Z.-Q. Qu, and R. P. Selvam, "Hybrid Expansion Method for Frequency Responses and their Sensitivities, Part II : Viscously Damped Systems," *Journal of Sound & Vibration,* V. 238, 369-388, 2000.
10. P. Vanhonacker, "Differential and Difference Sensitivities of Natural Frequencies and Mode Shapes of Mechanical Structures," *AIAA Journal,* V. 18, 1511-1514, 1980.
11. C. Yang, D. E. Adams, S.-W. Yoo, and H.-J. Kim, "An Embedded Sensitivity Approach for Diagnosing System-Level Noise and Vibration Problems," *Journal of Sound & Vibration*, accepted for publication, 2003.
12. C. Yang, D. E. Adams, S.-W. Yoo, and H.-J. Kim, "Embedded Sensitivity Functions for Structural Dynamic Systems," Proc. of the XXI International Modal Analysis Conference, 2003. **SlV**

The authors can be contacted at: yang21@purdue.edu and deadams@purdue.edu.